SOURCE CONTRIBUTIONS OF VOLATILE ORGANIC COMPOUNDS TO OZONE FORMATION IN SOUTHEAST TEXAS

Qi Ying*
Zachry Department of Civil Engineering, Texas A&M University, College Station, TX, USA

1. INTRODUCTION

The Houston-Galveston-Brazoria (HGB) and Beaumont-Port Arthur (BPA) areas in the southeast Texas are respectively in severe and moderate non-attainment status of the National Ambient Air Quality Standards for ozone (O_3) (EPA 2004) . Measures must be taken to control and further improve the O_3 air quality to better protect public health. To design an efficient emission control strategy, it is important to quantitatively determine which sources are responsible for O_3 formation in the polluted areas.

The major role of the VOCs in the O_3 formation process is in the formation of peroxy radicals that convert NO back to NO_2 and regenerate OH to allow sustained net O_3 formation (Finlayson-Pitts and Pitts 1997; Atkinson 2000). The objectives of this study are to 1) develop a source-oriented model to determine the contributions of VOCs from major emission sources to regional O_3 formation and 2) apply the model in Southeast Texas to determine source contributions to O_3 formation during a severe O_3 air pollution episode. This is the first time that the regional source contributions of VOCs to O_3 formation have been quantified using a three-dimensional source-oriented model.

2. METHOD

The net ozone formation can be attributed to responsible VOC sources based on the contributions of the VOCs and their intermediate oxidation products to the NO to NO_2 conversion process. In this study, the sources of the directly emitted VOCs, the reactive intermediates and the RO_2 and HO_2 radicals formed from their oxidation are properly tracked in the simulation of the photochemistry as well as transport and removal processes using a revised Community Multiscale Air Quality (CMAQ) model (version 4.6) with a source-oriented SAPRC-99 photochemical mechanism. The source-oriented technique introduces additional chemical species to represent contributions from different sources. For example, if superscript X represents VOC emissions from an explicit source X (for example, gasoline powered highway vehicles) and superscript O represents emissions from all other sources, then the reactions of a general reactive hydrocarbon (RH) from sources X and O with OH can be written as:

$$\begin{aligned} RH^X + OH &\rightarrow RO_2^X + H_2O \\ RH^O + OH &\rightarrow RO_2^O + H_2O \end{aligned} \qquad \text{(R1)}$$

In this way, the contribution of source X to the peroxy radical budget in the model can be directly determined. The amount of NO_2 that is regenerated through reactions of RO_2^X and NO at each chemistry time step can be determined by keeping track of the extent of reactions (R2) using the process analysis (PA) tool included in the standard CMAQ distribution.

$$\begin{aligned} RO_2^X + NO &\rightarrow NO_2 + RO^X \\ RO_2^O + NO &\rightarrow NO_2 + RO^O \end{aligned} \qquad \text{(R2)}$$

Similarly, by following the reactions of RO^X and RO^O with O_2, contributions to HO_2 for the two sources can be determined and the amount of NO_2 regenerated from HO_2 and NO reaction can be quantified.

The above discussion illustrates a method to track VOC from an explicit source (X) with emissions from other sources lumped into a single group (O). Theoretically, it is possible to expand the reactions so that emissions from more than one explicit source can be directly tracked simultaneously in a single model simulation. However the number of reactions in the expanded photochemical mechanism will increase almost exponentially due to the large amount of radical/radical reactions. In order to reduce the unnecessary complexity in expanding the mechanism and to make the approach more flexible to resolve a large number of sources, we decided to track only one source explicitly at a time. The final revised condensed SAPRC-99 mechanism includes 127 species and 489 reactions.

**Corresponding author:* Qi Ying, Texas A&M University, College Station, TX 77843-3136; e-mail: qying@civil.tamu.edu

3. MODEL APPLICATION

The CMAQ model with source-oriented SAPRC-99 extension was applied to study O_3 formation during the Texas Air Quality Study 2000 (TexAQS 2000) episode, from August 16 to September 6, 2000. A three-level nested domain was used in this study: the eastern United States was modeled with 36 km horizontal grid resolution; the east Texas and surrounding states were modeled with 12 km grid resolution and the HGB and BPA areas in southeast Texas were modeled with 4 km grid resolution (referred as the 4 km model domain hereafter).

Meteorology inputs needed to drive the CMAQ model were generated by the Meteorology-Chemistry Interface Processor (MCIP) using the output from the PSU/NCAR mesoscale model (MM5) simulation conducted by the Texas Commission of Environmental Quality. The EPA's 2001 Clean Air Interstate Rules (CAIR) emission inventory was used as a base to generate emission inputs for the TexAQS 2000 episode. The emission inventory was enhanced by using the episode-specific wildfire emissions from the Center for Energy and Environmental Resources at the University of Texas at Austin (Junquera, Russell et al. 2005). Emissions of olefins from petrochemical industrial point sources were increased by a factor of 5 from the reported values based on recent emission measurements. A revised Sparse Matrix Operator Kernel Emissions (SMOKE) emission processing model (version 2.4) from US EPA was used to process the updated CAIR emission inventory to generate gridded, speciated and temporally allocated VOC emission rates from each emission source for the CMAQ model. Biogenic emissions were generated using the Biogenic Emissions Inventory System, Version 3 (BEIS3) included in the SMOKE distribution. The 1-km resolution BELD3 land cover data with 230 different cover types (Vukovich and Pierce 2002) were used to estimate emission from vegetation.

The emissions were grouped into eight major source categories: biogenic sources, diesel vehicles, highway gasoline vehicles, off-highway gasoline vehicles, petroleum industries, other industries, solvent utilization and wildfires. Other VOC sources do not belong to these explicit source categories were lumped into the "other" source category. To generate emission for a specific source category, a Source Classification Code (SCC) filter was added to the SMOKE code so that only emissions from a set of predefined SCC codes would be processed.

4. RESULTS AND DISCUSSION

4.1 Predicted and Observed O_3 Concentrations

The predicted concentrations were compared with all available surface observation data. In general, results show that the predicted concentrations of O_3 and NOx agree well with observations. Peak O_3 concentrations in some days are under-predicted at several sites. This under-prediction of peak O_3 in the Houston area has also been previously reported in other modeling studies (Byun, Kim et al. 2006). Fig. 1 shows the comparison of the observed and predicted maximum 8-hour O_3 concentrations at all surface stations within the 4 km model domain. Except for several extreme events, the predictions are generally within 80-120% of the observed values.

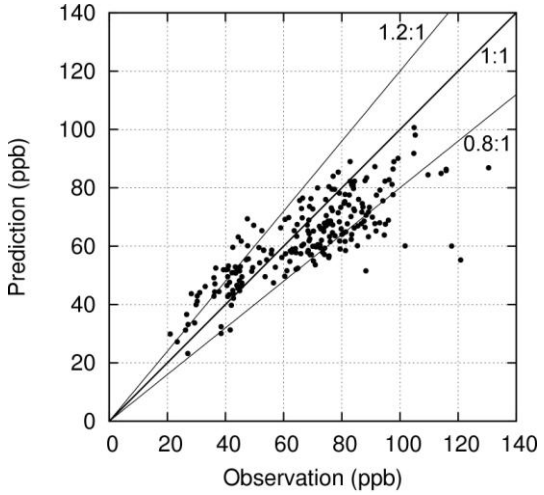

Fig. 1 Predicted and observed daily maximum 8-hour O_3 concentrations at individual observation station during the entire modeling episode.

4.2 Relationship between Net O_3 Formation and NO to NO_2 Conversion Rates

Fig. 2 shows the predicted NO to NO_2 conversion rates due to VOCs (the sum of the contributions from RO_2 and HO_2 radicals) for all grid cells and the corresponding net photochemical O_3 formation rates in the 4 km model domain. The net O_3 formation rate is the difference between the O_3 production rate and the O_3 removal rate in a gas-phase chemistry step. The results are for 1300-1400 Central Standard Time (CST), August 31, 2000 in the surface model layer (0-42 m from the surface). Results in upper layers are similar and thus are not shown here.

Only positive net O_3 formation rates are included in the plot. Grid cells where NOx concentrations are high actually show negative O_3 formation rates and these negative rates are not included in the plot. The data points are grouped into five different categories based on the VOC (ppbC) to NOx (ppb) ratio (VOC/NOx ratio) at each grid cell. In general, the net O_3 formation rate appears to be linearly correlated with the NO to NO_2 conversion rates. Data points deviated from this linear relationship usually have low VOC/NOx ratio of 0-5. The relatively higher NOx concentrations in these grid cells enhance the NO titration reaction with O_3 and lead to lower net O_3 formation rates (Kleinman, Daum et al. 2005). To achieve the highest O_3 formation rate, the VOC/NOx ratio has to be between 5 and 15. The excellent linear relationship between the NO to NO_2 conversion rate and the net O_3 formation rate for most of the data points within the domain at different VOC/NOx ratios suggests that it is reasonable to attribute the contributions of different VOC sources to net O_3 formation based on their contributions to the NO to NO_2 conversion processes.

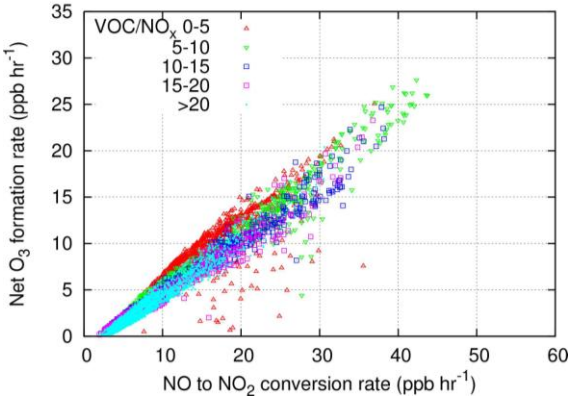

Fig. 2 Net ozone formation rate as a function of NO to NO_2 conversion rate due to peroxy radicals at 1300-1400 CST, August 31, 2000 for the surface model layer.

4.3 Source Contributions of VOC to Net O_3 Formation

The contributions of the i[th] VOC source to the net O_3 formation rate at a grid cell in the z[th] model layer is calculated using Equation (1) and (2):

$$\Delta O_{3,z}^{i} = f_z^{\,i} \cdot \Delta O_{3,z}\,\delta(\Delta O_{3,z}) \qquad (1)$$

$$f_z^{\,i} = \frac{R_{NO_2,z}^{i}}{\sum_{k=1}^{K} R_{NO_2,z}^{k}}, i = 1,2...K \qquad (2)$$

where superscript i is the source type index; z is the model layer index; $\Delta O_{3,z}$ is the predicted overall net O_3 formation rate (ppb hr^{-1}); $\Delta O_{3,z}^{i}$ is the apportioned contribution of VOC source i to the overall net O_3 formation rate (ppb hr^{-1}) and R_{NO_2} is the NO to NO_2 conversion rate (ppb hr^{-1}); f^i is the relative contribution of source i to the NO to NO_2 conversion. The delta function takes a value of 1 when the net O_3 formation rate is greater than zero otherwise it takes a value of 0. K is the total number of VOC sources.

O_3 formation in the layers above surface layer contributes to the surface ozone concentration through rapid vertical turbulent diffusion within the mixing layer (Byun, Kim et al. 2007; Song, Vizuete et al. 2008). Thus, it is useful to define a column-averaged source contribution expression as illustrated in Equation (3):

$$\Delta O_{3,avg}^{i} = \sum_{z=1}^{Z_{pbl}} w(z)\Delta O_{3,z}^{i} \qquad (3)$$

where $\Delta O_{3,avg}^{i}$ is the column-averaged contribution of source i to net ozone formation, Z_{pbl} is the layer where mixing layer height is located and the weighting function w(z) is the ratio of the thickness of the z[th] layer to the mixing layer height.

Fig. 3 shows the regional distribution of column-averaged net O_3 formation rate between 1300-1400 CST from August 16 to September 6, 2000. Highest O_3 formation rate of 16 ppb hr^{-1} is located in the downwind area of the urban and industrial regions in the model domain. In general, areas north of the Houston Ship Channel area show most significant O_3 formation rate at this hour. Several grid cells near the Ship Channel region shows low net O_3 formation rate. Further analysis of the results indicates that VOC/NOx ratios in these source areas are close to zero due to high NOx concentrations during daytime hours.

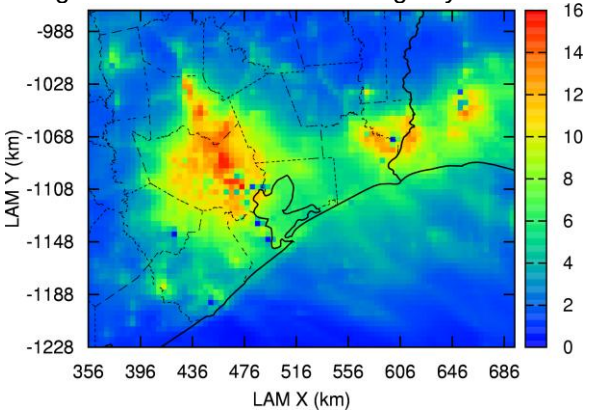

Fig. 3 Net ozone formation rate below the mixing height at 1300-1400 CST averaged from August 16 – September 6, 2000. Units are ppb hr^{-1}.

Fig. 4 shows the regional distribution of VOC source contributions to the column-averaged net O_3 formation rate at 1300-1400 CST averaged from 16 August to September 6, 2000 (see Fig. 3) based on equations (1-3). Fig. 4(a) shows that contribution from biogenic sources is highest in areas north of the Houston metropolitan area with a maximum net O_3 formation rate of approximately 12.2 ppb hr^{-1}. In the urban areas, the net O_3 formation rate due to biogenic sources is approximately 6 ppb hr^{-1}. The biogenic VOC concentrations are highest in areas near the northern boundary of the 4km domain but the O_3 formation rates are low due to low NOx concentrations (VOC/NOx ratio typically exceeds 500 in these areas). Fig. 4(b) shows that VOCs emitted from diesel vehicles do not contribute significantly to the net O_3 formation process. The highest contribution is approximately 0.1 ppb hr^{-1} in the urban Houston area. Fig. 4(c) shows that the spatial distribution of contributions from freeway gasoline vehicles is similar to that of diesel vehicle with highest contribution in the urban Houston region. The maximum net O_3 formation rate is approximately 2.5 ppb hr^{-1}. Fig. 4(d) shows that off-highway gasoline vehicles contribute to the net O_3 formation process with a maximum rate of approximately 1.4 ppb hr^{-1} in the Galveston and Port Arthur area. An inspection of the emission inventory indicates that emissions from pleasure marine crafts (boats powered by 2- and 4- stroke gasoline engines) are significant in these regions. Fig. 4(e) shows that petroleum industries contribute to a maximum of approximately 1.8 ppb hr^{-1} to the net photochemical O_3 formation process. The influence of the petroleum industries is obvious in the HGB and BPA areas as well as over the waters of the Galveston Bay and the Gulf of Mexico. Fig. 4(f) shows that other industrial sources contribute significantly to the O_3 formation processes with a peak value of 6.6 ppb^{-1} in the Ship Channel region. Fig. 4(g) shows that the contribution from solvent utilization is mainly located west part of the urban Houston region, with a maximum conversion rate of 1.4 ppb hr^{-1}. Fig. 4(h) shows that the influence of wildfires averaged over the entire model episode is only limited in a few areas with a highest contribution of approximately 1.2 ppb hr^{-1}. The actual contribution of a wildfire near the source is much higher than the episode average contribution shown here. Fig. 4(i) shows that sources unaccounted for by the above eight source categories contribute to the O_3 formation process mainly over the off-shore drilling areas in the Gulf of Mexico where the peak contribution can be as high as 3.1 ppb hr^{-1}. An inspection of the emission inventory indicates that emissions from reciprocating engines powered by natural gas are the most significant contributors to the "other" source categories in this area.

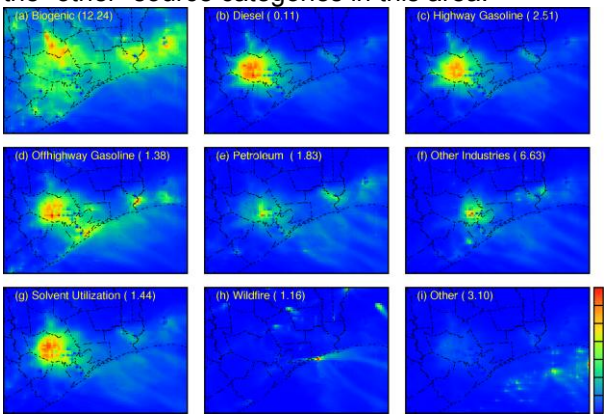

Fig. 4 Regional distributions of net photochemical ozone formation rates below the mixing height for 1300-1400 CST averaged from August 16 – September 6, 2000. The number on each panel is the maximum conversion rate for each source category in units of ppb hr^{-1}. The color bar on the right bottom can be used to estimate the rates on each sub-panel. The color scale is linear, starting from zero to the maximum value noted on the figure.

Fig. 5 shows the averaged hourly O_3 formation rate from August 16 to September 6, 2000 attributed to each VOC emission source. Top 10% of the air columns with highest column-averaged O_3 formation rate were included in the calculation. The highest column O_3 formation rate occurs at early afternoon hours. Contributions from anthropogenic sources are highest in the afternoon hours.

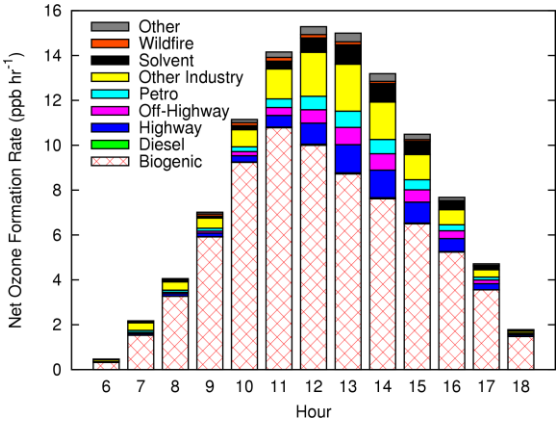

Fig. 5 Hourly VOC source contributions to net column ozone formation rate averaged from August 16 to September 7, 2000.

4.4 Back-trajectory Analysis of High O_3 Events

Although regional analysis discussed in the previous sections could determine VOC source contributions to O_3 formation rate at any given location at any given time, it does not directly determine which sources contribute to the observed O_3 concentration because O_3 builds up over time and the air parcel arrived at a specific receptor location passes through different regions with different emission signatures. Back-trajectories of air parcels arriving at locations when high O_3 concentrations occur can be used to better understand the sources that contribute to the elevated O_3 concentrations at specific locations. By investigating the O_3 concentrations, net O_3 formation rates and the source contributions of NO to NO_2 conversion along an air parcel trajectory, the contributions from major emission sources to a high O_3 event can be determined.

The relative contribution of VOCs from source i to surface O_3 concentration at the end of a trajectory can be calculated using Equation (4):

$$F^i = \frac{\sum_{t=1}^{T} d(t)\Delta O^i_{3,avg}(t)}{\sum_{k=1}^{K}\sum_{t=1}^{T} d(t)\Delta O^i_{3,avg}(t)}, i = 1,2,..., K \quad (4)$$

where F^i is the relative contribution to O_3 formation due to source i, $\Delta O^i_{3,avg}(t)$ is the contribution of source i to the column-averaged net O_3 formation rate at time t, as defined in Equation (3), T is the number of time steps used in the trajectory calculation, d(t) is a decay function that scales the contribution of O_3 formation at time t to the final O_3 concentration and K is the total number of VOC sources. In this study, d(t) is taken as 1 to simplify analysis. Analysis shows that this is good first approximation.

Equation (4) was applied to quantify the source contributions to the maximum 8-hour O_3 concentrations in the HGB and BPA areas. All the grid cells on land within the Texas state boundary in the 4 km domain were included in this analysis. For each grid cell, if the daily maximum 8-hour average O_3 concentration exceeds 90 ppb, 8 back-trajectories arriving at this grid cell during the 8-hour span were calculated and the contributions of VOCs to O_3 formation along each trajectory were determined. Although the 8-hour O_3 standard has been revised to 75 ppb, a cut concentration of 90 ppb is selected to represent extreme high O_3 exceedance cases. Most of the O_3 exceedance cases occur on August 25-31 and September 3-5, 2000. 300 grid cells were predicted to have daily maximum 8-hour O_3 concentration higher than the 90 ppb limit and thus a total number of 2400 trajectories were included in the analysis.

Fig. 6 shows the cumulative frequency distribution of the relative contributions of biogenic sources, internal combustion engines (diesel vehicles, highway gasoline vehicles, and off-highway gasoline vehicles combined), industries (petroleum industries and other industries combined), solvent utilization, wildfires and other sources to the net O_3 formation rate based on the 2400 10-hour trajectories. Biogenic sources are the major contributors to high O_3 concentrations for most of the 8-hour exceedance events predicted by the model. In approximately 50% of the cases biogenic sources contribute to over 55% of the net O_3 formation. Industrial sources and internal combustion engines are both significant anthropogenic source of VOC to O_3 formation. In approximately 50% of the cases, their respective contributions exceed 10% and in approximately 20% of the cases their contributions exceed 30%. Solvent utilization is also a large anthropogenic source, contributing over 10% for 20% of the cases considered. Maximum relative vehicle contribution to O_3 formation is approximately 20%. Contributions from wildfires vary significantly. In some cases, its contribution can be as high as 34%, exceeding the maximum contribution from solvent utilization.

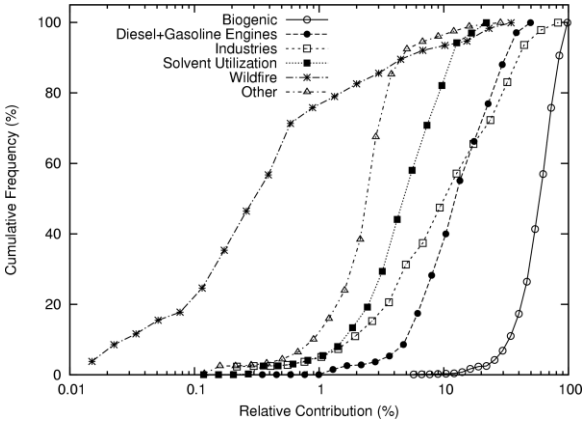

Fig. 6 Cumulative frequency distribution of the relative VOC source contributions to net ozone formation for surface grid cells where predicted daily maximum 8-hour average ozone concentration is greater than 90 ppb.

5. SUMMARY

In this paper, we illustrated that during the TexAQS 2000 O_3 episode, the net photochemical O_3 formation rate was linearly related with the NO

to NO_2 conversion rate due to peroxy and hydroperoxy radicals generated from the photochemical oxidation of VOCs. A source-oriented SAPRC-99 photochemical mechanism was developed and incorporated into the CMAQ model to directly determine the contributions of eight explicit VOC sources to the predicted net O_3 formation in the entire model domain based on their contributions to the NO to NO_2 conversion rate. Of the eight sources studied, biogenic sources were found to be the largest contributor to regional O_3 formation. Industrial sources are the largest anthropogenic source to O_3 formation, followed by gasoline vehicles and solvent utilization. Wildfires could contribute to fast ozone formation near the fire locations but their influence is generally localized.

ACKNOWLEDGEMENTS

This research is supported by the Texas Air Research Center (TARC) under the project 078ATM2080A.

REFERENCES

Atkinson R (2000) Atmospheric chemistry of VOCs and NOx. Atmospheric Environment. 34(12-14):2063-2101.

Byun DW, et al. (2006) Evaluation of air quality models for the simulation of a high ozone episode in the Houston metropolitan area. Atmospheric Environment. 41(4):837-853.

Byun DW, et al. (2007) Evaluation of air quality models for the simulation of a high ozone episode in the Houston metropolitan area. Atmospheric Environment. 41(4):837-853.

EPA: 2004, Region 6: State Designations for the 1997 8-Hour Ozone Standard (http://www.epa.gov/ozonedesignations/1997standards/regions/region6desig.htm)

Finlayson-Pitts BJ and Pitts JN (1997) Tropospheric air pollution: Ozone, airborne toxics, polycyclic aromatic hydrocarbons, and particles. Science. 276(5315):1045-1052.

Junquera V, et al. (2005) Wildfires in eastern Texas in August and September 2000: Emissions, aircraft measurements, and impact on photochemistry. Atmospheric Environment. 39(27):4983-4996

Kleinman LI, et al. (2005) A comparative study of ozone production in five U.S. metropolitan areas. J. Geophys. Res.-Atmos. 110(D2):20.

Song J, et al. (2008) Comparisons of modeled and observed isoprene concentrations in southeast Texas. Atmospheric Environment. 42(8):1922-1940.

Vukovich JM and Pierce T (2002) The Implementation of BEIS3 within the SMOKE modeling framework. 2002, / MCNC-Environmental Modeling Center, Research Triangle Park and National Oceanic and Atmospheric Administration, City.